Catalysis Letters (2024) 154:2841–2851
https://doi.org/10.1007/s10562-023-04535-4

Selective Catalytic Oxidation of Ammonia over Cr-Ce Mixed Oxide Catalysts in the Presence of Sulfur Dioxide

Fangyuan Zhou[1] · Xiaoqiang Wang[1,2,3] · Li Sun[2] · Ruiwen Jia[2] · Yue Liu[1] · Zhongbiao Wu[1]

Received: 9 September 2023 / Accepted: 18 November 2023 / Published online: 26 December 2023

Abstract

In this paper, the influence of SO_2 on the performances of selective catalytic oxidation (SCO) of NH_3 on Cr-Ce mixed oxide catalysts had been disclosed. Experimental results revealed that the existence of SO_2 could greatly suppress the unselective catalytic oxidation of ammonia over Cr-Ce mixed oxide catalysts with strong redox capacity, though the ammonia conversion rate was somewhat lowered after SO_2 introduction. As such, near or above 90% ammonia conversion and excellent N_2 selectivity within 350–450 °C could be achieved on $Cr_{10}Ce$ sample after 20 h reaction running in the presence of 350 ppm SO_2. Characterization results indicated that SO_2 could induce the formation of surface sulfates on $Cr_{10}Ce$ catalysts and enhance its surface acidity, which would inhibit the over-oxidation of NH_3. More importantly, the bulk-like sulfation of $Cr_{10}Ce$ samples was damped in the presence of SO_2 compared to pure CeO_2, which allowed certain active oxygens participating in NH_3-SCO reaction. DFT results also confirmed that the adsorbed SO_2 would preferentially interact with the oxygens around the interface of CeO_2 and Cr_2O_3, thereby preventing the retained active oxygens from being further sulfation. Therefore, the Cr-Ce mixed oxide catalysts showed promising application potential for eliminating NH_3 slip downstream NH_3-SCR process.

Graphical abstract

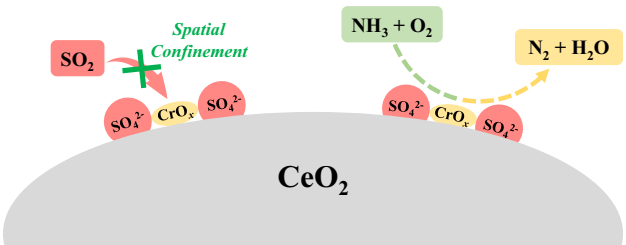

Keywords Cr-Ce mixed oxide catalysts · NH_3-SCO · Ammonia slip · Sulfur dioxides

1 Introduction

As the "haze promoter", ammonia (NH_3) has been included as a controlled indicator of air pollutants, which caused tremendous concerns on ecological environment and human health [1–5]. Apart from industrial production procedure, stock farming and agricultural fertilization, one of the primary sources of ammonia emissions is the ammonia slip during the industrial flue gas denitrification process when ammonia is used as reductant [6–9]. Owing to fluctuation of gaseous distribution and operational condition, over stoichiometric ratio of NH_3 had been injected to ensure the

✉ Yue Liu
yueliu@zju.edu.cn

1 Department of Environmental Engineering, Zhejiang University, 866 Yuhangtang Road, Hangzhou 310058, People's Republic of China

2 Jiehua Holdings Co., LTD, 3 Jinji Road, Haining 314419, People's Republic of China

3 College of Biological, Chemical Science and Engineering, Jiaxing University, 899 Guangqiong Road, Jiaxing 314001, People's Republic of China

deNO$_x$ efficiency during selective catalytic reduction (SCR) or selective non-catalytic reduction (SNCR) process, resulting in the emission of unreacted NH_3 so-called ammonia slip [10, 11]. The NH_3 slip would lead to the plug in the downstream air-preheater and form secondary inorganic aerosols [11].

Nowadays, the NH_3-SCO (selective catalytic oxidation of NH_3) catalyst installed at the tail-end of SCR units could be one promising way to solve the NH_3 slip problem [2]. Commonly, the NH_3-SCO reactions follow the internal SCR mechanism (i-SCR), which can be described as follows: the absorbed ammonia on catalysts is partly oxidized to NO_x and the resulted NO_x then reacts with NH_3 to produce N_2 and H_2O [12, 13]. Generally, an excellent NH_3-SCO catalyst should possess suitable redox ability, which could not only meet the requirement of deeply dehydrogenation of NH_3 but also suppress the over-oxidation to avoid the formation of byproducts, including N_2O, NO and NO_2.

The most studied NH_3-SCO catalysts included noble-metal based catalysts and transition metal-based catalysts [12, 13]. Although possessing excellent low-temperature NH_3-SCO activity, noble-metal based catalysts with narrow temperature window could be hardly affordable in slip-NH_3 control application [12, 14]. As for transition metal-based catalysts, Cu-based catalysts had attracted lots of researchers' attention owing to the relatively well activity and N_2 selectivity [12, 15]. However, the coexistence of gaseous SO_2 in the flue gas is inevitable, which would exert serious deactivation effect on NH_3-SCO activity due to the strong interaction between Cu active phase and SO_2 [10, 16, 17].

In the previous literatures, chromic (Cr) based catalysts with excellent redox ability and exceptional resistance to sulfur and chlorine species, owing to its low interaction with HCl/SO_2 [18, 19], had been widely reported in NH_3-SCR [19–21], NO oxidation [22] and VOCs catalytic combustion [18, 23, 24], etc. Additionally, due to good oxygen storage capacity, CeO_2 has been often applied as promoter or main active phase in NH_3-SCR/SCO reactions [25–28]. Moreover, based on our previous works [29, 30], CeO_2 could serve as the sacrificial sites to promote the SCR performance of Cu or Mn based catalysts in the presence of SO_2. As such, the Cr-Ce mixed oxide catalysts might be one promising candidate to achieve well NH_3-SCO performances, where the well redox capacity of Cr-Ce catalyst could effectively activate NH_3 and sulfation would also provide acidic sites to inhibit the over-oxidation of NH_3. However, what happens to the NH_3-SCO performance of Cr-Ce mixed oxide catalysts in the presence of SO_2 needs to be further investigated.

Therefore, in this manuscript, to deal with the challenges of NH_3 slip elimination, the Cr-Ce mixed oxide catalysts prepared by impregnation method were employed to investigate their activities and stabilities in the presence of SO_2 and H_2O during NH_3-SCO reaction process. Additionally, various characterizations and density functional theory (DFT) simulations were then conducted to reveal the inherent mechanism for NH_3-SCO reaction behaviors over Cr-Ce mixed oxide catalysts.

2 Experimental Section

Firstly, pure Cr_2O_3 and CeO_2 catalysts were prepared by the direct calcination of nitrate precursors. Then, various Cr-Ce mixed oxide catalysts were synthesized by impregnating $Cr(NO_3)_3{\cdot}9H_2O$ on previous obtained CeO_2 support. And the obtained Cr-Ce mixed oxide catalysts were denoted as Cr_xCe, where x represented Cr/Ce molar ratio ($x = 1$–20%). Moreover, the selected $Cr_{10}Ce$ catalyst after stability tests in the presence of 350 ppm SO_2 at 350 °C were denoted as $Cr_{10}Ce\text{-}U_y$, where y represented the duration of stability tests period ($y = 10$, 20 and 30 h). To investigate the intrinsic mechanism of SO_2 influence on NH_3-SCO performances, the samples before and after stability tests were subjected to various characterizations to disclose. And more detailed experimental illustration and computational method were given in the *Supporting Information*.

3 Results and Discussion

3.1 Catalytic Performances

The NH_3-SCO performances of various fresh Cr_xCe mixed oxide catalysts were depicted in Fig. 1. As shown in Fig. 1a, fresh CeO_2 sample hardly converted ammonia efficiently within the investigated temperature window, while 100% NH_3 conversion in the temperature range of 250–450 °C was achieved on pure Cr_2O_3. Unsurprisingly, NH_3 oxidation activity of Cr_xCe catalysts lied between that of pure Cr_2O_3 and CeO_2 samples. And the addition of Cr significantly promoted NH_3 conversion of CeO_2, where the NH_3 conversion changed little when Cr/Ce ratio exceeded 10%. The well dispersion of Cr species owing to the interaction between Cr species and CeO_2 could account for it. However, high amount of N_2O and NO_x species generated on Cr_xCe catalysts at low-medium and medium–high temperature range respectively, which resulted in rather poor N_2 selectivity on all Cr-related samples (see Figs. 1b and S1). It could be due to the fact that Cr_xCe samples with strong redox ability but lack of surface acidity promoted the unselective oxidation of ammonia [13]. Moreover, $Cr_{10}Ce$ sample with approximative NH_3 conversion and relative higher N_2 selectivity compered to pure Cr_2O_3 was further applied in the investigation of the effect of SO_2.

As shown in Fig. 1c, in the presence of 350 ppm SO_2 at 350 °C, $Cr_{10}Ce$ sample achieved complete NH_3 conversion

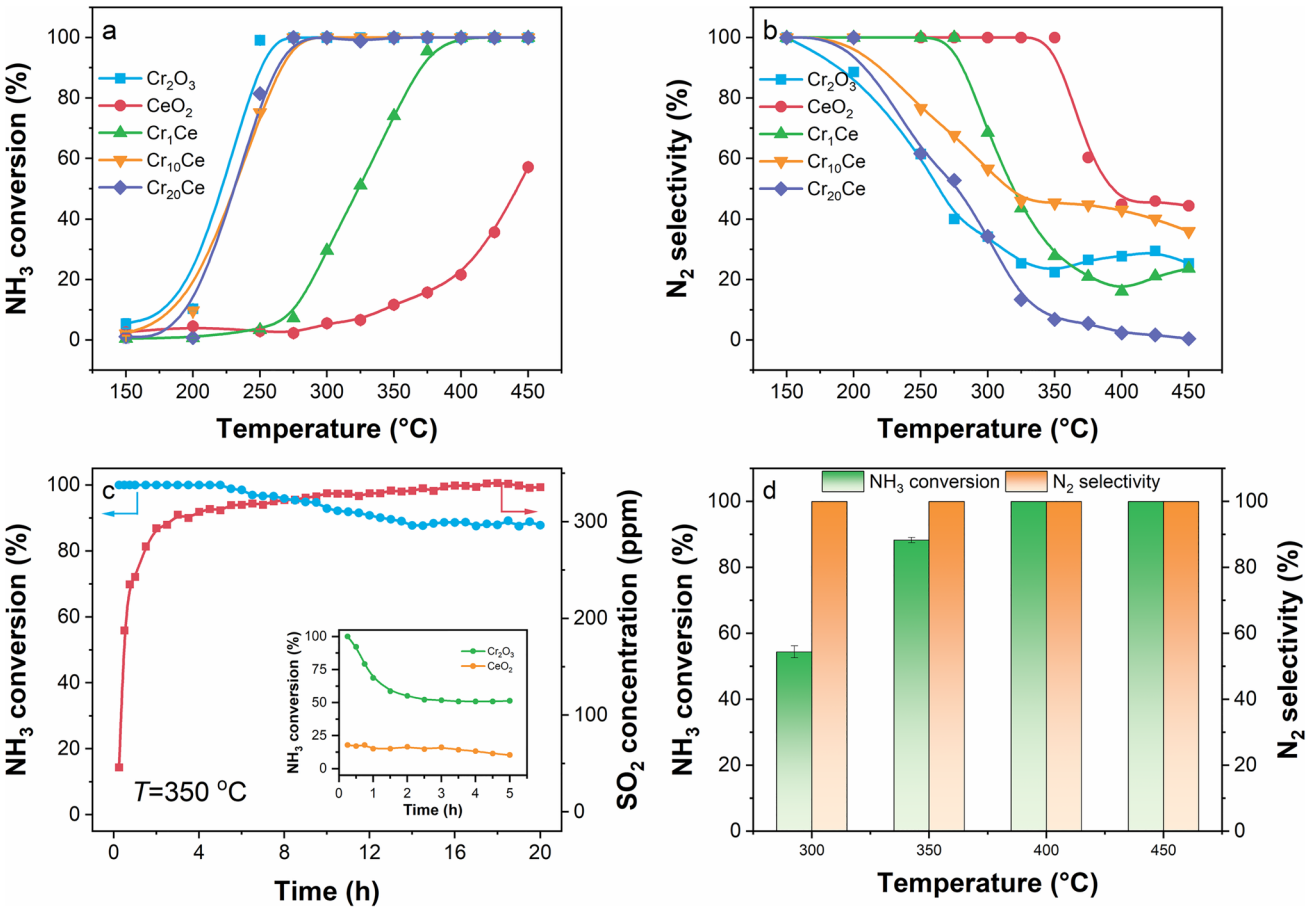

Fig. 1 NH_3 conversion (**a**) and N_2 selectivity (**b**) of various samples; NH_3 conversion and outlet SO_2 concentration during SO_2 resistance stability tests of $Cr_{10}Ce$ sample at 350 °C (**c**); NH_3-SCO performance of $Cr_{10}Ce$ sample after 20 h SO_2 poisoning reaction running under different temperature (**d**). NH_3-SCO reaction conditions: $[NH_3]=100$ ppm, $[O_2]=[H_2O]=5$ vol.%, $[SO_2]=350$ ppm (if applicable), N_2 balance

during the initial 5 h, but gradually decreased to about 88% NH_3 conversion for the next 8 h and then maintained at this value for the later reaction time. In comparison, the introduction of SO_2 would quickly decrease NH_3 conversion of pure Cr_2O_3 from 100% to around 50%. The evolution in NH_3 oxidation activity was in good accordance with that of outlet SO_2 concentration detected, where it increased gradually to finally reached its inlet value in the final stage of tests. This observation indicated that the deposition of sulfur could somewhat lower the NH_3 oxidation activity, as sulfation of metal oxides by SO_2 would generally deteriorate their redox capacity [31, 32]. However, such poisoning effect was lessened greatly on $Cr_{10}Ce$ sample compared to pure Cr_2O_3, which deserved to be further investigation regarding the intrinsic mechanism. In addition, the NH_3-SCO performances of $Cr_{10}Ce$ sample after 20 h SO_2 poisoning under different temperature had also been investigated (see Fig. 1d). It could be seen that $Cr_{10}Ce$ sample possessed near or above 90% NH_3 conversion and 100% N_2 selectivity in the temperature range of 350–450 °C. Therefore, Cr-Ce mixed oxides could be suitable candidate of NH_3 slip elimination catalysts downstream SCR units. It was noted that the existence of SO_2 slightly decreased NH_3 conversion of $Cr_{10}Ce$ sample but significantly promoted N_2 selectivity at temperatures higher than 350 °C. For instance, N_2 selectivity of $Cr_{10}Ce$ sample at 350 °C increased from less than 50% to 100%. Therefore, the existence of SO_2 could greatly suppress the unselective catalytic oxidation of ammonia over Cr-Ce mixed oxide catalysts. And the promoted N_2 selectivity in the SO_2 stability tests might be attributed to the enhanced surface acidity but weakened redox ability with surface sulfation, where similar findings had been mentioned in previous works [31, 33]. To reveal the related mechanism regarding the effect of SO_2 on NH_3-SCO performances, various corresponding characterizations were conducted in the following sections.

3.2 The Physical Property Changes

To identify the physical property changes of Cr-Ce mixed oxide catalysts caused by SO_2, the specific surface area, XRD and TEM/SEM characterizations had been conducted. As illustrated in Tables 1 and S1, a S_{BET} of 69 m^2/g was obtained on fresh CeO_2 sample, and that decreased at an elevated molar ratio of Cr/Ce for fresh Cr_xCe samples. The introduction of certain Cr species into micro-channels of CeO_2 during preparation process could be responsible for that [25]. Furthermore, after stability tests in the presence of SO_2, the surface area of $Cr_{10}Ce$ sample would be deteriorated over time (from 57 m^2/g of fresh $Cr_{10}Ce$ to 41 m^2/g of $Cr_{10}Ce$-U_{30}), owing to the blockage effect derived from the formed sulfate species [31, 32]. Additionally, as shown in Figs. 2 and S2a, XRD patterns of various samples showed that various diffraction peaks located at 28.6°, 33.1°, 47.5°, 56.3°, 59.1°, 69.4°, 76.7°, 79.1° and 88.4° emerged, which could be assigned to CeO_2 with cubic fluorite structure [PDF#43–1002]. However, characteristic diffraction peaks related to Cr species were hardly detected for $Cr_{10}Ce$ sample, indicating the high dispersion of Cr species [21, 34]. Furthermore, the intensity of characteristic diffraction peaks of $Cr_{10}Ce$-U_y samples gradually decreased compared to fresh $Cr_{10}Ce$ sample, demonstrating that the crystal structure of CeO_2 was damaged by SO_2 poisoning. And similar findings could be observed for CeO_2-U_{20} and Cr_2O_3-U_{20} samples (see Fig. S2b), however, it was found that better crystallinity of Cr_2O_3 reserved after SO_2 resistance stability tests than CeO_2. It might be implied that SO_2 would preferentially interact on surface Ce sites to form cerium sulfate species compared to Cr species during stability tests, which had been similarly reported in the previous work [17].

In addition, the morphology and microstructure of fresh $Cr_{10}Ce$ and selected $Cr_{10}Ce$-U_{20} samples were studied by TEM and SEM. As shown in Figs. 3 and S3, no obvious lattice stripes of Cr related crystals were found in $Cr_{10}Ce$ sample, suggesting the well dispersion of Cr species on CeO_2 support, which was consistent with XRD patterns. Furthermore, slightly blurred edges of crystals were observed on $Cr_{10}Ce$-U_{20} sample, indicating that the sulfation of catalysts occurred after SO_2 introduction in NH_3-SCO reaction [35]. As illustrated in Table S2, elements distribution analyzed by SEM EDS-Mapping indicated that there deposited certain amount of sulfur (S) species on $Cr_{10}Ce$-U_{20} sample, while the content of surface O, Ce, Cr and nitrogen (N) species did not show evident changes compared to fresh $Cr_{10}Ce$ sample. The above phenomena indicated that the metal oxides sulfation but not ammonium sulfates accumulation is the main cause of sulfur deposition on $Cr_{10}Ce$-U_{20} catalyst [31].

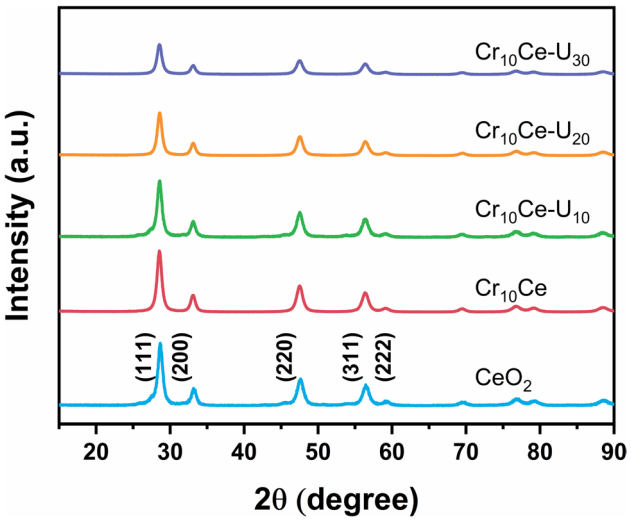

Fig. 2 XRD patterns of CeO_2 and various $Cr_{10}Ce$ related samples

3.3 The Redox Ability and Surface Acidity Changes

To investigate the changes in the redox ability of different samples before and after stability tests in the presence of SO_2, H_2-TPR and O_2-TPD experiments were conducted and the results were presented in Fig. 4. As seen the H_2-TPR results in Fig. 4a, the pristine CeO_2 sample showed two reduction peaks of surface-active oxygen species related to ceria at 406 °C and 523 °C, respectively. After Cr addition, the reduction peaks shifted to a lower temperature range (349 °C and 445 °C), indicating the promoted reducibility derived from Cr species. Based on the previous works [19, 34], the two peaks could be ascribed to the reduction of Cr^{6+} to Cr^{3+} and active surface oxygen derived from Cr–O-Ce strong interactions, respectively. However, after reaction with SO_2 poisoning, the reduction peaks of various samples shifted to higher temperature range (592 °C for CeO_2-U_{20}, 450 and 556 °C for $Cr_{10}Ce$-U_{20}), indicating the suppressed reducibility of catalysts caused by sulfation. As reported in the literatures [36, 37], the much stronger H_2 consumption peaks emerged at above 550 °C on the two samples were subjected to the reduction of formed sulfate species. And the relatively lower reduction temperature of sulfate species observed on $Cr_{10}Ce$-U_{20} sample compared to

Table 1 BET surface areas and pore structures of various catalysts

Samples	$Cr_{10}Ce$	$Cr_{10}Ce$-U_{10}	$Cr_{10}Ce$-U_{20}	$Cr_{10}Ce$-U_{30}
Specific surface area (m^2/g)	57	45	42	41
Total pore volume (cm^3/g)	0.16	0.16	0.13	0.12
Average pore diameter (nm)	10.92	12.54	12.55	12.63

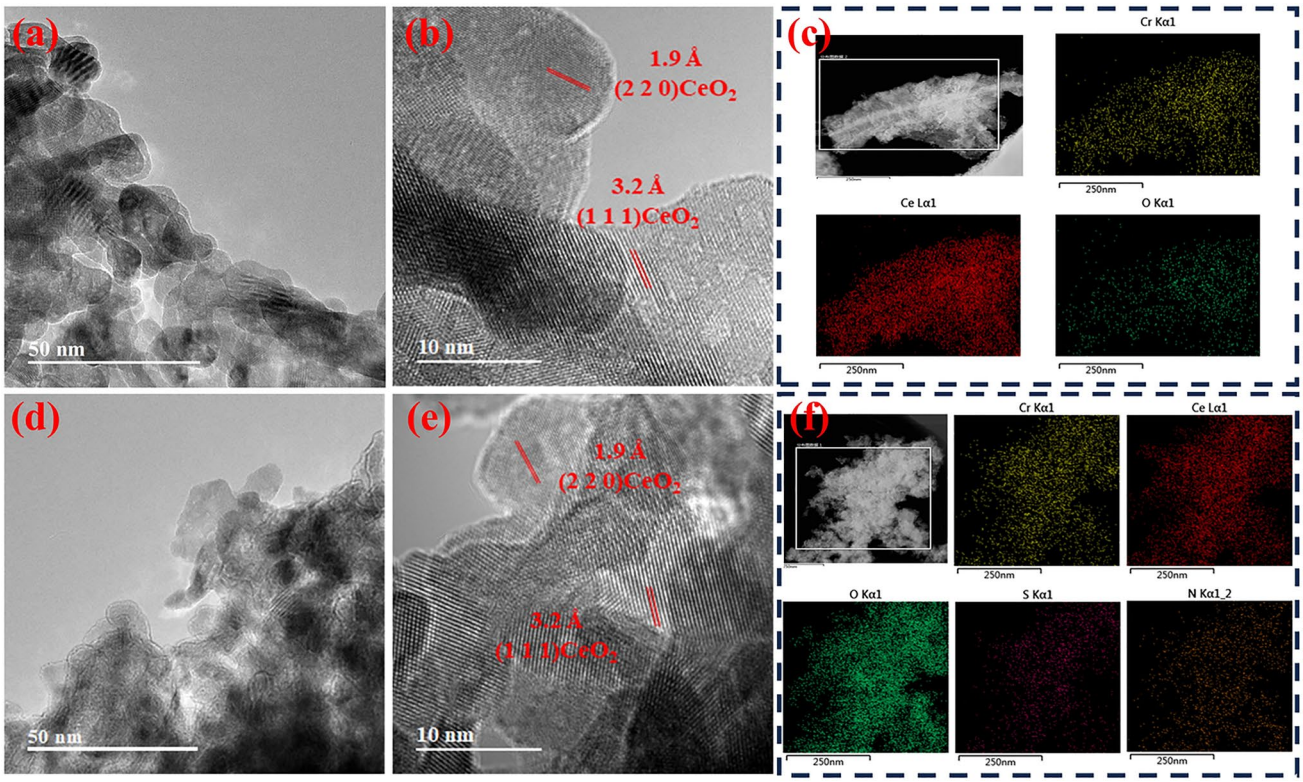

Fig. 3 TEM, HR-TEM and EDS-mapping images of $Cr_{10}Ce$ (**a**, **b**, **c**) and $Cr_{10}Ce\text{-}U_{20}$ (**d**, **e**, **f**) samples

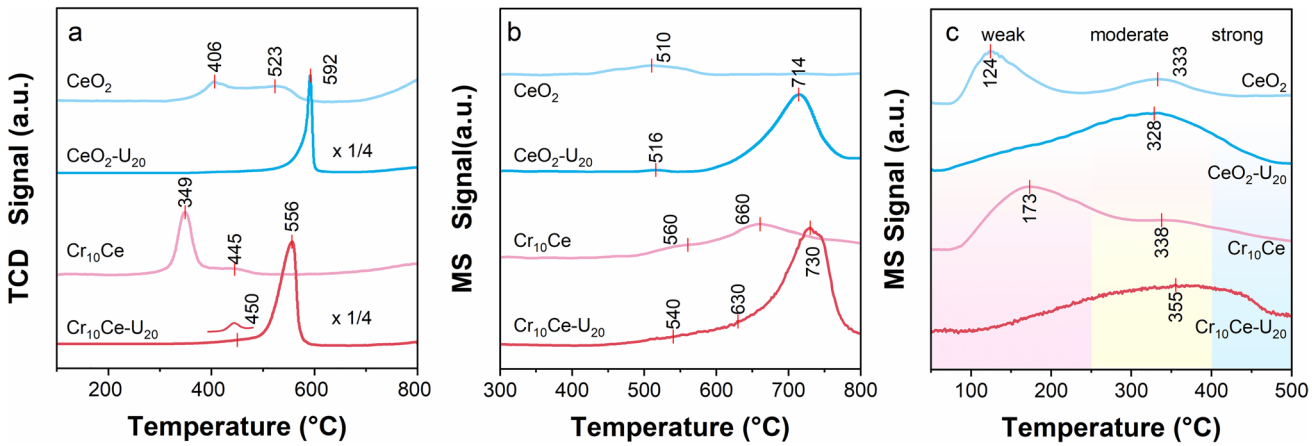

Fig. 4 H_2-TPR (**a**), O_2-TPD (**b**) and NH_3-TPD (**c**) profiles of various samples

$CeO_2\text{-}U_{20}$ sample suggested that Cr addition would decrease the stability of sulfate species on CeO_2. Notably, compared with $CeO_2\text{-}U_{20}$ sample, one small peak for the reduction of Cr-Ce species at 450 °C still could be found on $Cr_{10}Ce\text{-}U_{20}$ sample. It could be concluded that sulfation could not completely eliminate the active oxygens in $Cr_{10}Ce$ sample and the reserved active oxygens were still capable to participate in the NH_3 oxidation reaction. And the O_2-TPD results shown in Fig. 4b further confirmed this conclusion.

From Fig. 4b, one small oxygen desorption peak at 510 °C could be seen on fresh CeO_2 sample, where $Cr_{10}Ce$ catalyst showed two stronger oxygen desorption peaks at 560 and 660 °C. As mentioned [31, 37], the much larger oxygen desorption peak of $Cr_{10}Ce$ sample indicated that the formed strong Cr-Ce interactions could bring about abundant active oxygen species (O_β), inducing better activation ability of reactants during NH_3-SCO reaction process. After reaction with SO_2, $CeO_2\text{-}U_{20}$ sample showed

one oxygen desorption peak at about 714 °C, while three oxygen desorption peaks located at 540, 630 and 730 °C emerged on $Cr_{10}Ce$-U_{20} sample. Excluding these dramatically increased oxygen desorption peaks above 700 °C caused by thermal decomposition of sulfate species [31, 37], $Cr_{10}Ce$-U_{20} sample could maintain more active oxygen species to participate in SCO reaction after SO_2 introduction, which was in accordance with the H_2-TPR results.

Figure 4c showed the NH_3-TPD profiles of various samples. From the previous works [38, 39], the desorption peaks of NH_3 could be divided into three sections within 50–250 °C, 250–400 °C and 400–500 °C, corresponding to NH_3 desorbed from weak, moderate and strong acidic sites, respectively. It could be found that SO_2 poisoning significantly enlarged the amount of the moderate/strong acidic sites of catalysts. It was reasonable that the sulfate species formed were of strong electronic attractive effect, which improved the surface acidity [36]. It was widely recognized that strong acidity could inhibit the over oxidation of ammonia in SCR reaction [40]. Therefore, the enhanced surface acidity after SO_2 poisoning was account for the improved N_2 selectivity of $Cr_{10}Ce$ sample for NH_3-SCO reaction in the presence of SO_2 (see Fig. 1).

3.4 The Influence of SO_2 on Surface Chemical States

To further reveal the influences of SO_2 on the existence states of surface elements in the catalyst, various $Cr_{10}Ce$ samples before and after stability tests in the presence of SO_2 were subjected to XPS characterization (see Fig. 5). The surface atomic concentration distribution and detailed peak calculation results were given in Table 2. As shown, the characteristic peaks of Cr 2p XPS spectra could be deconvoluted into three categories, including Cr^{6+} (~ 578.7 eV for Cr $2p_{3/2}$ and ~ 588.4 eV for Cr $2p_{1/2}$), Cr^{3+} (~ 576.8 eV for Cr $2p_{3/2}$ and ~ 586.4 eV for Cr $2p_{1/2}$) and Cr^{2+} (~ 575.8 eV for Cr $2p_{3/2}$ and ~ 585.8 eV for Cr $2p_{1/2}$) [21, 41], while the Ce 3d XPS spectra were divided into two categories (u for Ce^{4+} and v for Ce^{3+}) [33, 42, 43]. Compared with fresh $Cr_{10}Ce$ sample, positive shifts in the binding energy of Cr 2p and Ce 3d XPS peaks could be observed after SO_2 poisoning. The strong electronic interaction of sulfate groups could be ascribed to the main reason for that [44]. However, the shift in Cr 2p and Ce 3d XPS peaks showed respective variations in different durations of SO_2 poisoning reaction. It was evident that the displacement of Cr 2p XPS peaks occurred solely within the initial 10 h of SO_2 poisoning reaction, whereas the deviation in Ce 3d XPS peaks mainly occurred in the

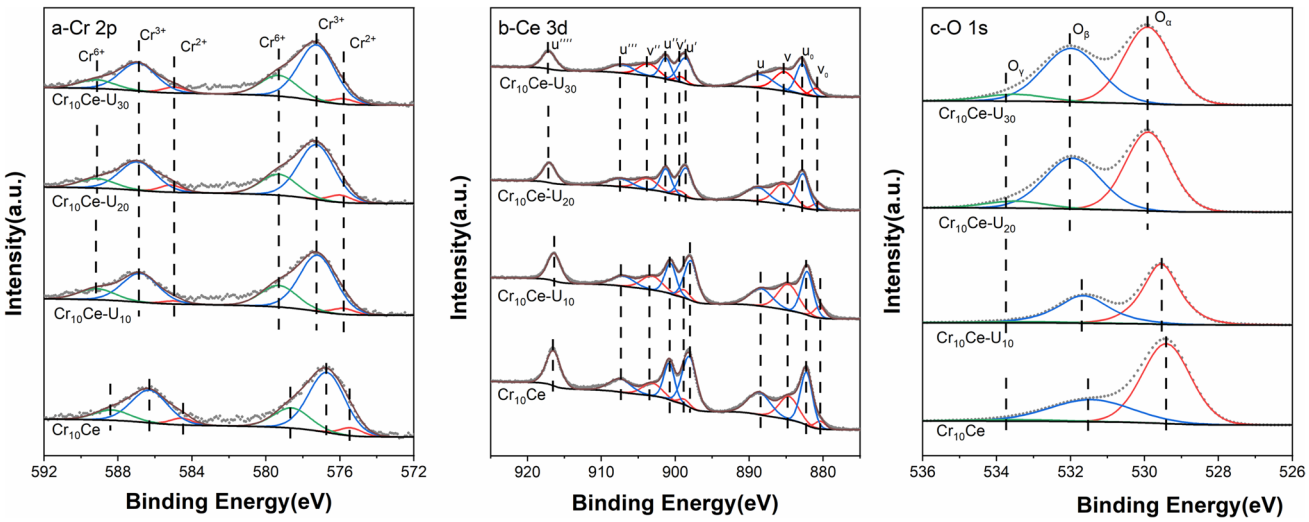

Fig. 5 The Cr 2p (**a**), Ce 3d (**b**) and O 1 s (**c**) XPS spectra of various samples

Table 2 Surface atomic concentration and peak calculation results by XPS analysis

Samples	Surface atomic concentration (%)					O_β/O	Ce^{3+}/Ce	Cr species		
	Cr	Ce	O	N	S			Cr^{2+}	Cr^{3+}	Cr^{6+}
$Cr_{10}Ce$	6.04	14.63	79.33	/	/	31.35	21.20	5.87	70.41	23.72
$Cr_{10}Ce$-U_{10}	4.81	9.26	77.82	2.25	5.86	34.09	28.69	7.81	65.61	26.58
$Cr_{10}Ce$-U_{20}	4.78	8.28	78.66	2.12	6.16	41.50	29.79	5.68	68.11	26.22
$Cr_{10}Ce$-U_{30}	4.49	7.95	78.39	2.39	6.78	42.90	30.42	4.25	69.74	26.00

$Cr_{10}Ce\text{-}U_{20}$ sample. It was suggested that the impact of SO_2 poisoning on Cr species diminished over time, while it progressively affected Ce species.

Furthermore, focusing on the changes in the subpeaks of Cr and Ce species on various $Cr_{10}Ce\text{-}U_y$ samples, it could be seen that the proportion of Cr^{6+}/Cr_{total} changed little except the increase during the initial 10-h reaction time, while Ce^{3+}/Ce_{total} ratio continued to increase. The above results indicated that the presence of SO_2 would significantly affect the existence states of Ce, whereas the impact on Cr was somewhat mitigated, which agreed with the results related to locations of XPS peaks. The increase of Ce^{3+}/Ce_{total} resulted from the reduction effect caused by SO_2 and the initial increase of Cr^{6+}/Cr_{total} might be due to the electronic interaction with sulfate species [31]. From Fig. 5c, the O 1 s spectra of the catalysts were fitted into three sub-peaks: lattice oxygen (O_α, 528.6–530.0 eV), surface chemisorbed oxygen species (O_β, 531.4–532.0 eV) and oxygen containing surface groups (O_γ, 532.6–533.5 eV) like carbonate and/or hydroxyl species [29, 43]. As listed in Table 2, SO_2 poisoning reaction would promote the formation of surface chemisorbed oxygen species derived from surface formed sulfate species [29]. Notably, the O_β/O_{total} in $Cr_{10}Ce\text{-}U_y$ samples trended to be stable when the reaction time increased beyond 20 h, indicating that the sulfation became lessened, corresponding to its stable NH_3-SCO activity. Additionally, the above findings of weakened sulfation process were further confirmed by various N 1s and S 2p XPS spectra (see Fig. S4 and Table 2), as the obvious increased S and N species only occurred within the initial 10 h of SO_2 poisoning reaction. Furthermore, the surface atomic concentration of S was about 2.5 times higher than that of N on various $Cr_xCe\text{-}U_y$ samples. It was implied that sulfate species existed as metal sulfate species rather than ammonium sulfates on the samples after stability tests.

3.5 Reaction Process Analysis

To identify the reaction process of NH_3-SCO, TPSR studies had been also carried out on $Cr_{10}Ce$ sample before and after 20 h SO_2 poisoning. As shown in Fig. 6, it could be seen that the ammonia could be converted on fresh $Cr_{10}Ce$ sample at relative low temperature (about 250 °C), where less N_2 emission and higher amount of NO emerged compared to $Ce_{10}Ce\text{-}U_{20}$ sample. It was implied that the activation of NH_3 could occur on $Cr_{10}Ce$ sample easily but mainly follow the unselective catalytic oxidation process. After 20 h reaction running in the presence of SO_2, owing to the suppressed redox ability and enhanced surface acidity, the ammonia conversion onset temperature of $Ce_{10}Ce\text{-}U_{20}$ sample shifted to higher temperature range (about 300 °C), where the signals of released byproducts, including N_2O, NO and NO_2, obviously decreased, indicating the achievement of well N_2 selectivity. The above results were in accordance with the previous obtained redox ability, surface acidity and activity test results.

3.6 SO_2 Influential Mechanism Analysis

Based on the SEM EDS-mapping results above, it was indicated that less ammonium sulfates accumulated on catalysts after SO_2 poisoning reaction running. Therefore, TP, FT-IR and TG analysis were further conducted to identify it. As shown in Fig. S5, no signals of NO, H_2O and N_2 species derived from NH_4HSO_4 decomposition and only SO_2 emission due to sulfate species dissociation could be detected on the $Cr_{10}Ce\text{-}U_{20}$ sample. Then, FT-IR experiments in Fig. S6

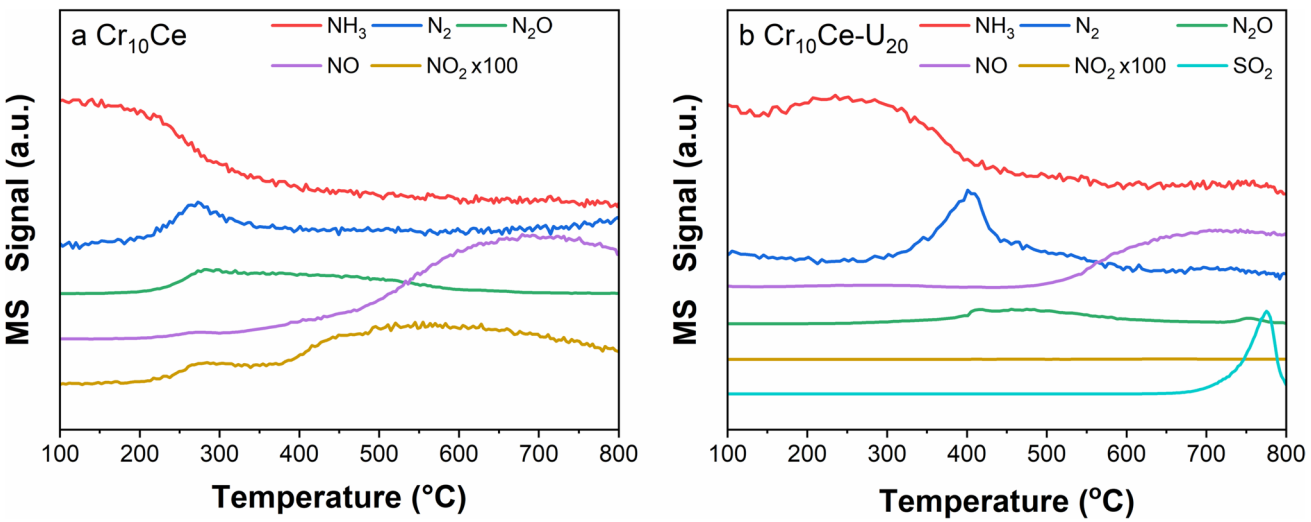

Fig. 6 NH_3+O_2 -TPSR profiles of $Cr_{10}Ce$ (**a**) and $Cr_{10}Ce\text{-}U_{20}$ (**b**) samples

indicated that almost no characterization peaks ascribed to NH_4^+ existed on $Cr_{10}Ce\text{-}U_{20}$ sample [38]. Finally, from TG analysis in Fig. S7, $Cr_{10}Ce\text{-}U_{20}$ sample did not show obvious weight loss at around 300 °C, where the temperature was related to the decomposition of NH_4HSO_4 [30, 45]. As such, it could be concluded that sulfur deposition on $Cr_{10}Ce\text{-}U_{20}$ sample was mainly sulfate species associated with metal cations.

Aiming to investigate the existences of sulfate species on $Cr_{10}Ce$ sample, SO_2-TPD and SO_2+O_2 DRIFT experiments were conducted (see Fig. 7). From SO_2-TPD results in Fig. 7a, it could be observed that only one SO_2 desorption peak emerged on Cr_2O_3, $Cr_{10}Ce$ and CeO_2 samples, which located at 651, 721 and 735 °C, respectively. Obviously, the desorption peak area of sulfate species on various samples decreased as follows: $Cr_2O_3 << Cr_{10}Ce < CeO_2$, indicating that Cr addition diminished the formation of sulfate species and its stability on CeO_2. Although it was found that the sulfation of pure Cr_2O_3 was least severe among three samples, it lost about half of its activity by SO_2 poisoning at 350 °C. As such, the sulfur aversion feature of Cr species could not explain the high NH_3-SCO activity of $Cr_{10}Ce$ sample during the reaction in the presence of SO_2, whose inherent reason need to be further clarified. In addition, DRIFT studies had been performed to further elucidate the states of adsorbed sulfate species. As shown in Fig. 7b, after exposure to 500 ppm SO_2+5 vol% O_2 at 350 °C for 1 h, various peaks located at 1624 (1618), 1520, 1402 ~ 1382, 1314 ~ 1273, 1170, 1032 and 956 cm^{-1} emerged, which could be ascribed to H_2O (1624 ~ 1618 cm^{-1}), pyrosulfate species (1520 cm^{-1}), surface sulfate species (1402 ~ 1382 cm^{-1}) and bulk-like sulfate species (1314 ~ 1273, 1170, 1032 and 956 cm^{-1}), respectively [31, 32]. Although surface and bulk-like sulfate species were detected on various samples, the $Cr_{10}Ce$ sample exhibited a majority formation of surface sulfate species, whereas CeO_2 sample predominantly generated bulk-like sulfate species. Based on previous literatures [37, 46], the bulk-like sulfate species usually possessed more harmful effect on the activity compared to surface sulfate species, which would greatly inhibit the redox cycle of Cr-Ce species. These results indicated that Cr addition significantly suppressed the deep sulfation of bulk phase in $Cr_{10}Ce$ sample, which should be the main reason of its well activity against SO_2 poisoning. Moreover, little sulfate species formed on $Cr_{10}Ce\text{-}U_{20}$ sample was indicative of the saturation point being reached in the adsorption of SO_2, which was related to its stable activity.

DFT studies were then performed to explore the intrinsic reason of such phenomena (see Fig. 8 and Table 3). The adsorption energies of SO_2 molecule at atop Ce and O sites on the CeO_2 surface were − 0.28 and − 1.40 eV, while that at atop Ce, O_1 (Ce-O-Ce), O_2 (Cr-O-Ce) and Cr sites on the Cr-doped CeO_2 surface were − 0.83, − 1.93, − 1.66 and − 1.69 eV, respectively. It was confirmed that the SO_2 preferred to bond with the O atoms of Ce-O-Ce model around Cr atoms compared to pure Ce-O-Ce model. It could explain that the sulfation of Ceria was more serious and prolonged compared with that of Cr species. As such, during the NH_3-SCO reaction, the adsorbed SO_2 would preferentially interact with the oxygens around the interface of CeO_2 and Cr_2O_3. Different with the final deactivation of $CuCeO_x$ after SO_2 introduction reported in the literature [17], CrO_x possessed stronger aversion to SO_2 than Cu species, combined with the spatial protection effect of the formed sulfate species on the interface of CeO_2 and Cr_2O_3 [47], further SO_2 poisoning on Cr_2O_3 could be greatly inhibited. Therefore, remained clean Cr species and active oxygens could still participate in the NH_3-SCO reaction, which had been verified

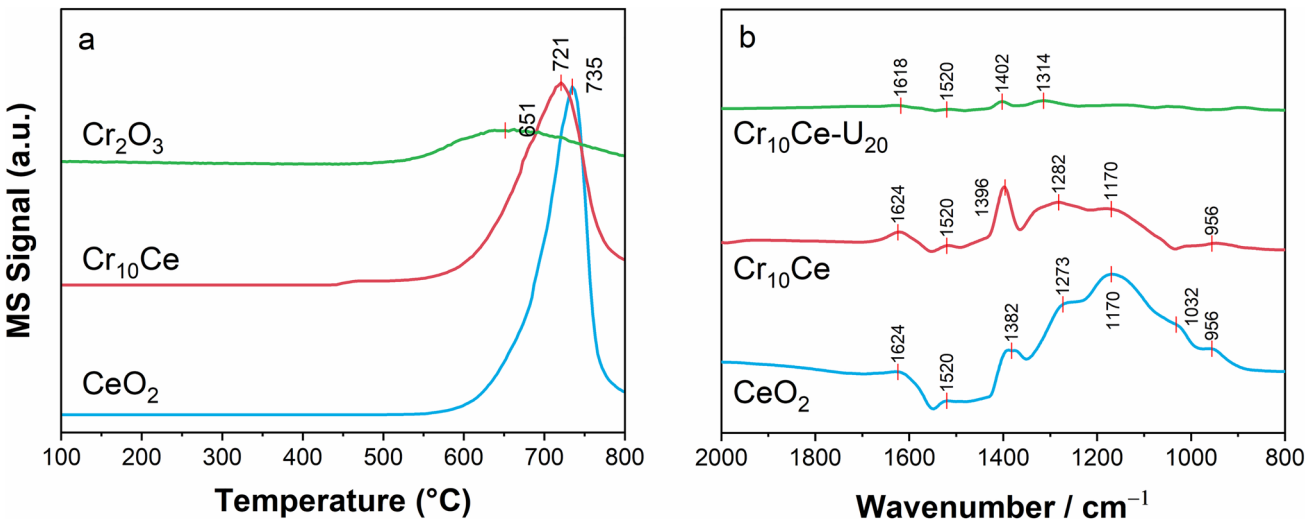

Fig. 7 SO_2-TPD (**a**) and in situ DRIFT spectra of SO_2+O_2 co-adsorption (**b**) over various samples

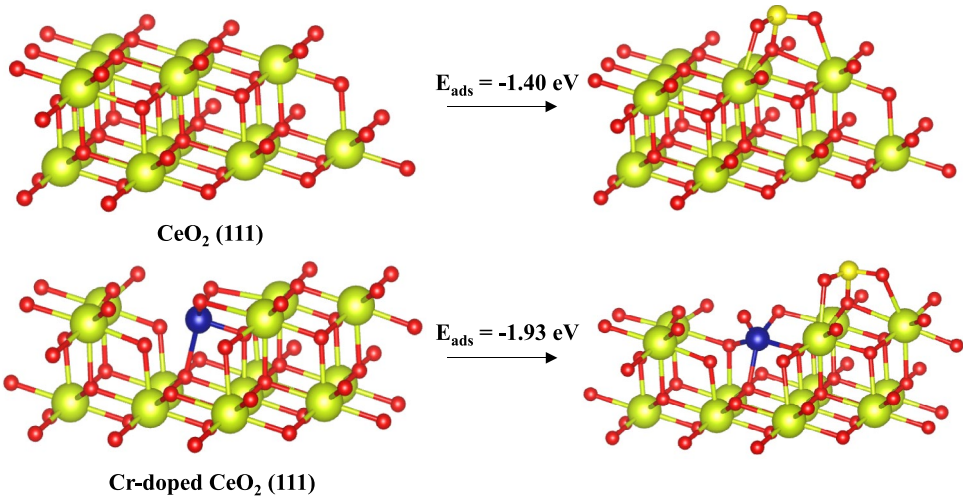

Fig. 8 Optimized SO_2 molecule adsorption on CeO_2 and Cr-doped CeO_2 models

Table 3 SO_2 adsorption formation energy results by DFT simulation

	Sites (CeO_2)	E_{ads} (eV)	Sites (Cr-doped CeO_2)	E_{ads} (eV)
SO_2 molecule adsorption	top Ce	− 0.28	top Ce	− 0.83
	top O_1(Ce-O-Ce)	− 1.40	top O_1(Ce-O-Ce)	− 1.93
	/	/	top O_2(Cr-O-Ce)	− 1.66
	/	/	top Cr	− 1.69

by H_2-TPR and O_2-TPD results in Fig. 4. This should be the main reason of superior SCO performances achieved on $Cr_{10}Ce$ mixed oxide catalyst in the presence of SO_2.

4 Conclusion

In summary, the influence of SO_2 on NH_3-SCO performance of Cr-Ce mixed oxide catalysts had been disclosed. The existence of SO_2 in flue gases would somewhat inhibit the NH_3 oxidation ability due to the formation of surface sulfation but still could guarantee the fulfilled NH_3-SCO reaction at high temperatures. In addition, the N_2 selectivity was greatly improved due to the enhanced acidity. For instance, near or above 90% ammonia conversion with excellent N_2 selectivity in the temperature range of 350–450 °C could be achieved on $Cr_{10}Ce$ sample after 20 h reaction running in the presence of 350 ppm SO_2, while pure Cr_2O_3 quickly lost half of its activity. SO_2 would preferentially attack the oxygens around the interface of CeO_2 and Cr_2O_3 in Ce-Cr mixed oxides, the formed surface sulfate species created a protection structure for preventing the further sulfation of the metal oxides. As such, certain amount of active oxygens and clean Cr species were remained to fulfill the NH_3-SCO reaction. Therefore, robust NH_3-SCO performances in the presence of SO_2 could be achieved on $Cr_{10}Ce$ sample, which showed promising application potential for eliminating NH_3 slip downstream NH_3-SCR process.

Supplementary Information The online version contains supplementary material available at https://doi.org/10.1007/s10562-023-04535-4.

Acknowledgements The authors acknowledge for the financial support of National Key R&D Program of China (No. 2022YFC3701600), National Natural Science Foundation of China (No. 22276162 and 22306072) and China Postdoctoral Science Foundation (No. 2023M731441).

Declarations

Conflict of interest There are no conflicts to declare.

References

1. Liu Y, Liu Z, Wang C, Xu J, Ai J, Liu X, Zhang A, Zhao Y, Du C, Shan B (2023) Unraveling the lattice O assisted internal selective catalytic reduction mechanism on high N_2 selectivity of CuO_x/PtCu catalysts in NH_3-SCO. ACS Catal 13:7178–7188
2. Wang H, Murayama T, Lin M, Sakaguchi N, Haruta M, Miura H, Shishido T (2022) Understanding the distinct effects of Ag nanoparticles and highly dispersed Ag species on N_2 selectivity in NH_3-SCO reaction. ACS Catal 12:6108–6118
3. Amblard M, Burch R, Southward BWL (2000) An investigation of the selective oxidation of NH_3 to N_2 in gasified biomass in the presence of excess CO and H_2 using zeolite catalysts. Catal Lett 68:105–108
4. Fung WK, Claeys M, van Steen E (2012) Effective utilization of the catalytically active phase: NH_3 oxidation over unsupported and supported Co_3O_4. Catal Lett 142:445–451

5. Ono Y, Wakita H, Inui T (1998) Relationship between oxidation states of copper supported on alumina and activities for catalytic combustion of NH_3. Catal Lett 53:83–89
6. Wang H, Lin M, Murayama T, Feng S, Haruta M, Miura H, Shishido T (2021) Ag size/structure-dependent effect on low-temperature selective catalytic oxidation of NH_3 over Ag/MnO_2. ACS Catal 11:8576–8584
7. Liao Y, Liu Z, Li Z, Gao G, Ji L, Xu H, Huang W, Qu Z, Yan N (2022) The unique CO activation effects for boosting NH_3 selective catalytic oxidation over CuO_x-CeO_2. Environ Sci Technol 56:10402–10411
8. Sun D, Liu Q, Liu Z, Gui G, Huang Z (2009) An in situ DRIFTS study on SCR of NO with NH_3 Over V_2O_5/AC surface. Catal Lett 132:122–126
9. Xiao X, Xiong S, Li B, Geng Y, Yang S (2016) Role of WO_3 in NO reduction with NH_3 over V_2O_5-WO_3/TiO_2: a new insight from the kinetic study. Catal Lett 146:2242–2251
10. Yu Y, Wei D, Tong Z, Wang J, Chen J, He C (2022) Rationally engineered ReO_x-$CuSO_4$/TiO_2 catalyst with superior NH_3-SCO efficiency and remarkably boosted SO_2 tolerance: synergy of acid sites and surface adsorbed oxygen. Chem Eng J 442:136356
11. Zhang Y, Zhang M, Zang Y, Wang H, Liu C, Wei L, Wang Y, He L, Wang W, Zhang Z, Han R, Ji N, Song C, Lu X, Ma D, Sun Y, Liu Q (2023) Elimination of NH_3 by interfacial charge transfer over the $Ag/CeSnO_x$ tandem catalyst. ACS Catal 13:1449–1461
12. Gao F, Liu Y, Sani Z, Tang X, Yi H, Zhao S, Yu Q, Zhou Y (2021) Advances in selective catalytic oxidation of ammonia (NH_3-SCO) to dinitrogen in excess oxygen: a review on typical catalysts, catalytic performances and reaction mechanisms. J Environ Chem Eng 9:104575
13. Li Z, Wang C, Qiu J, Ma Y, Wang C, Sun X, Li K, Ning P, Wang F (2023) Advances in selective catalytic oxidation of ammonia (NH_3-SCO): a review of catalyst structure-activity relationship and design principles. Chin Chem Lett 108432
14. Lan T, Zhao Y, Deng J, Zhang J, Shi L, Zhang D (2020) Selective catalytic oxidation of NH_3 over noble metal-based catalysts: state of the art and future prospects. Catal Sci Technol 10:5792–5810
15. Jabłońska M (2020) Progress on selective catalytic ammonia oxidation (NH_3-SCO) over cu-containing zeolite-based catalysts. ChemCatChem 12:4490–4500
16. Chen C, Cao Y, Liu S, Jia W (2020) The effect of SO_2 on NH_3-SCO and SCR properties over Cu/SCR catalyst. Appl Surf Sci 507:145153
17. Li Z, Chen J, Jiang M, Li L, Zhang J, Duan W, Wen J, Wang H, Liu M, Zhang Q, Chen J, Ning P (2022) Study on SO_2 poisoning mechanism of CO catalytic oxidation reaction on copper-cerium catalyst. Catal Lett 152:2729–2737
18. Su J, Yao W, Liu Y, Wu Z (2017) The impact of CrO_x loading on reaction behaviors of dichloromethane (DCM) catalytic combustion over Cr-O/HZSM-5 catalysts. Appl Surf Sci 396:1026–1033
19. Guo M, Liu Q, Zhao P, Han J, Li X, Ha Y, Fu Z, Song C, Ji N, Liu C, Ma D, Li Z (2019) Promotional effect of SO_2 on Cr_2O_3 catalysts for the marine NH_3-SCR reaction. Chem Eng J 361:830–838
20. Liu H, Wei L, Yue R, Chen Y (2010) CrO_x-CeO_2 binary oxide as a superior catalyst for NO reduction with NH_3 at low temperature in presence of CO. Catal Commun 11:829–833
21. Guo M, Liu Q, Liu C, Wang X, Bi Y, Fan B, Ma D, Liang X, Li Z (2021) Rational design of novel $CrZrO_x$ catalysts for efficient low temperature SCR of NO_x. Chem Eng J 413:127554
22. Cai W, Zhao Y, Chen M, Jiang X, Wang H, Ou M, Wan S, Zhong Q (2018) The formation of 3D spherical Cr-Ce mixed oxides with roughness surface and their enhanced low-temperature NO oxidation. Chem Eng J 333:414–422
23. Su J, Liu Y, Yao W, Wu Z (2016) Catalytic combustion of dichloromethane over HZSM-5-supported typical transition metal (Cr, Fe, and Cu) oxide catalysts: a stability study. J Phys Chem C 120:18046–18054
24. Fei X, Ouyang W, Gu Z, Cao S, Wang H, Weng X, Wu Z (2021) Effect of Cr doping in promoting the catalytic oxidation of dichloromethane (CH_2Cl_2) over Cr-Co@Z catalysts. J Hazard Mater 413:125327
25. Wang X, Liu Y, Ying Q, Yao W, Wu Z (2018) The superior performance of Nb-modified Cu-Ce-Ti mixed oxides for the selective catalytic reduction of NO with NH_3 at low temperature. Appl Catal A 562:19–27
26. Wang X, Liu Y, Wu Z (2021) Temperature-dependent influencing mechanism of carbon monoxide on the NH_3-SCR process over ceria-based catalysts. ACS ES&T Eng 1:1131–1139
27. Liu W, Long Y, Liu S, Zhou Y, Tong X, Yin Y, Li X, Hu K, Hu J (2022) Promotional effect of Ce in NH_3-SCO and NH_3-SCR reactions over Cu-Ce/SCR catalysts. J Ind Eng Chem 107:197–206
28. Yan T, Chen J, Li K, Yin R, Peng Y, Li J (2023) CeO_2/α-MnO_2 nanorods as dual-functional catalyst for simultaneous abatement of nitric oxide and chlorobenzene. Catal Lett
29. Gu T, Liu Y, Weng X, Wang H, Wu Z (2010) The enhanced performance of ceria with surface sulfation for selective catalytic reduction of NO by NH_3. Catal Commun 12:310–313
30. Jin R, Liu Y, Wang Y, Cen W, Wu Z, Wang H, Weng X (2014) The role of cerium in the improved SO_2 tolerance for NO reduction with NH_3 over Mn-Ce/TiO_2 catalyst at low temperature. Appl Catal B 148–149:582–588
31. Wang X, Liu Y, Yao W, Wu Z (2019) Boosting the low-temperature activity and sulfur tolerance of $CeZr_2O_x$ catalysts by antimony addition for the selective catalytic reduction of NO with ammonia. J Colloid Interface Sci 546:152–162
32. Wang X, Liu Y, Wu Z (2019) Highly active $NbOPO_4$ supported Cu-Ce catalyst for NH_3-SCR reaction with superior sulfur resistance. Chem Eng J 382:122941
33. Yao W, Liu Y, Wu Z (2018) The promoting effect of CeO_2@Ce-O-P multi-core@shell structure on SO_2 tolerance for selective catalytic reduction of NO with NH_3 at low temperature. Appl Surf Sci 442:156–163
34. Xue L, Wei N, Zhao C, Hu X, Yun J, Chen Z, Deng Z, Chen Z (2022) Promotion effect of Cr addition on the activity and SO_2 tolerance of CeO_x catalysts for the NH_3-SCR at middle-low temperature. J Energy Inst 105:472–480
35. Qi K, Yi Q, Fang D, Gong P, Shi L, Gao L, Li X, He F, Xie J (2023) Temperature dependence of reaction mechanisms and SO_2 tolerance over a promising monolithic CuY catalyst for NO removal. Appl Surf Sci 615:156473
36. Yang S, Guo Y, Chang H, Ma L, Peng Y, Qu Z, Yan N, Wang C, Li J (2013) Novel effect of SO_2 on the SCR reaction over CeO_2: mechanism and significance. Appl Catal B 136–137:19–28
37. Wang X, Liu Y, Wu Z (2020) The poisoning mechanisms of different zinc species on a ceria-based NH_3-SCR catalyst and the co-effects of zinc and gas-phase sulfur/chlorine species. J Colloid Interface Sci 566:153–162
38. Chi R, Wang X, Liu Y, Wu Z (2023) Highly active alkali etching silica-modified Cu-Ce-Ti catalyst with superior water resistance for low temperature NO_x reduction. Appl Surf Sci 627:157304
39. Wang X, Zhu Y, Liu Y, Weng X, Wu Z (2022) Tailoring the simultaneous abatement of methanol and NO_x on Sb-Ce-Zr catalysts via copper modification. Front Environ Sci Eng 16:130
40. Liu F, Asakura K, He H, Shan W, Shi X, Zhang C (2011) Influence of sulfation on iron titanate catalyst for the selective catalytic reduction of NO_x with NH_3. Appl Catal B 103:369–377
41. Guo M, Liu C, Liu Q, Wang Y, Fan B, Wang H, Liu B, Cui S, Zhao Y (2022) Investigation of SO_2 resistance on Novel $Cr_{0.8}Zr_{0.2}O_x$ catalysts for marine low-temperature SCR of NO removal. ACS ES&T Eng 2:1825–1835

42. Yao W, Wang X, Liu Y, Wu Z (2019) Ce-O-P material supported CeO_2 catalysts: a novel catalyst for selective catalytic reduction of NO with NH_3 at low temperature. Appl Surf Sci 467–468:439–445
43. Liu Y, Yao W, Cao X, Weng X, Wang Y, Wang H, Wu Z (2014) Supercritical water syntheses of Ce_xTiO_2 nano-catalysts with a strong metal-support interaction for selective catalytic reduction of NO with NH_3. Appl Catal B 160–161:684–691
44. Ying Q, Liu Y, Wang N, Zhang Y, Wu Z (2020) The superior performance of dichloromethane oxidation over Ru doped sulfated TiO_2 catalysts: synergistic effects of Ru dispersion and acidity. Appl Surf Sci 515:145971
45. Guo K, Fan G, Gu D, Yu S, Ma K, Liu A, Tan W, Wang J, Du X, Zou W, Tang C, Dong L (2019) Pore size expansion accelerates ammonium bisulfate decomposition for improved sulfur resistance in low-temperature NH_3-SCR. ACS Appl Mater Interfaces 11:4900–4907
46. Zhang L, Li L, Cao Y, Yao X, Ge C, Gao F, Deng Y, Tang C, Dong L (2015) Getting insight into the influence of SO_2 on TiO_2/CeO_2 for the selective catalytic reduction of NO by NH_3. Appl Catal B 165:589–598
47. Costa CN, Savva PG, Fierro JLG, Efstathiou AM (2007) Industrial H_2-SCR of NO on a novel Pt/MgO-CeO_2 catalyst. Appl Catal B 75:147–156